EVS30 Symposium
Stuttgart, Germany, October 9 - 11, 2017

Thermal abuse of Lithium-ion batteries: Combined study by experiments and simulation

Carlos Ziebert[1], Andreas Melcher[1], Wenjiao Zhao[1], Magnus Rohde[1], Hans Jürgen Seifert[1]

[1]*Institute of Applied Materials - Applied Materials Physics, Karlsruhe Institute of Technology, Carlos.Ziebert@kit.edu*

Summary

Several exothermic reactions can occur as the inner temperature of a Lithium-ion cell is increasing during thermal abuse. If the heat generation is larger than the dissipated heat to the surroundings, this leads to heat accumulation in the cell and acceleration of the reactions, which can end up in a thermal runaway. In this work the thermal abuse of 18650 cells has been studied both experimentally and by simulations. Commercial cells were exposed to external heating in an Accelerating Rate Calorimeter. The Heat-Wait-Seek and the Ramp Heating method were applied. If an exothermal reaction is detected, the system switches to the adiabatic mode, which means that the temperature of the calorimeter follows instantaneously the surface temperature of the cell, i.e. the cell cannot exchange heat with the surroundings anymore. Thus it is heating up more and more until the thermal runaway occurs.

In order to simulate the abuse mechanisms, the coupled electrochemical-thermal model based on porous electrode theory has been extended with exothermic contributions coming from side reactions that follow an Arrhenius law. These extensions have been modeled with a constant fuel model and implemented into COMSOL Multiphysics® using the *Battery and Fuel Cell* Module coupled to the *Heat Transfer in Solids* Module. The spatial overall mean cell temperature during the time evolution of a thermal runaway has been computed. Moreover the different stages of the thermal runaway have been classified. Finally the simulation results have been compared with the experimental results from the ARC tests. By such combined studies cooling systems of electric vehicles can be better adjusted and safety can be increased.

Keywords: lithium battery, simulation, thermal management, battery model, battery management

1 Introduction

Lithium-ion batteries (LIBs) have found a wide range of applications in the last three decades, like notebooks, cell phones, power tools or hybrid or fully electric vehicles. The thermal runaway of a LIB is the worst case scenario which must be avoided under all circumstances. Several exothermic reactions can occur as the inner cell temperature is increasing during thermal abuse. If the heat generation is larger than the dissipated heat to the surroundings, this leads to heat accumulation in the cell and acceleration of the

chemical reactions, which can end up in a thermal runaway if the point of no return has been overcome. In these terms, a thermal runaway describes a rapid temperature increase in a very short time interval of the typical order of 100K/min and above. Thus it is of outmost importance to get a deeper insight into the underlying processes. Calorimetry of the electrochemical cells and their individual active materials represents a versatile method to obtain quantitative thermal and thermodynamic data. The accelerating rate calorimeter (ARC) is the instrument of choice, because it can also be used for safety tests where the cell is driven up to the thermal runaway [1], because it is robust and especially designed to withstand even an explosion of the cell. An ARC provides a safe and adiabatic environment for the in-operando study of the cells. In an adiabatic environment no heat exchange between the sample and the surroundings is possible, so that the heat energy of reactions can be monitored by the measured temperature change.

In parallel to the experiments, applying a simulation approach promises a deeper theoretical understanding of the occurring phenomena inside the LIB. The standard multi-scale multi domain (MSMD) models developed in [2, 3], that are based on porous electrode theory [4], cannot simulate the thermal runaway. First improvements are reported by Hatchard et al. in [5], where the heat equation is coupled with ordinary differential equations (ODEs), describing the exothermic reactions based on an Arrhenius-type law. Spotnitz et al. and Peng et al. give first partial differential equation (PDE) based models of the thermal runaway including reaction kinetics based on an ODE formulation [6, 7].

In this work the thermal abuse of 18650 cells has been studied both experimentally and by simulations. In the experiments commercial cells were exposed to external heating in an ARC and either the Heat-Wait-Seek method or the ramp heating method was applied to drive the cells up to thermal runaway. From the resulting temperature vs temperature rate plots the related reaction mechanisms could be investigated quantitatively. For the simulations a similar approach as presented by Peng et al.[6] has been used in this work and has been implemented into COMSOL Multiphysics® (version 5.2) using the *Battery and Fuel Cell* Module coupled to the *Heat Transfer in Solids* Module. Using this model the spatial overall mean cell temperature during the time evolution of a thermal runaway has been computed and the different thermal runaway stages have been classified.

2 Experimental Details

Commercial 18650 cells have been studied in an accelerating rate calorimeter (es-ARC, THT Company, s. Fig. 1a)) using both the Heat-Wait-Seek (HWS) method and the ramp heating (RH) method [8]. The principles of ARC operation can be explained using the schematic setup shown in Fig. 1b).

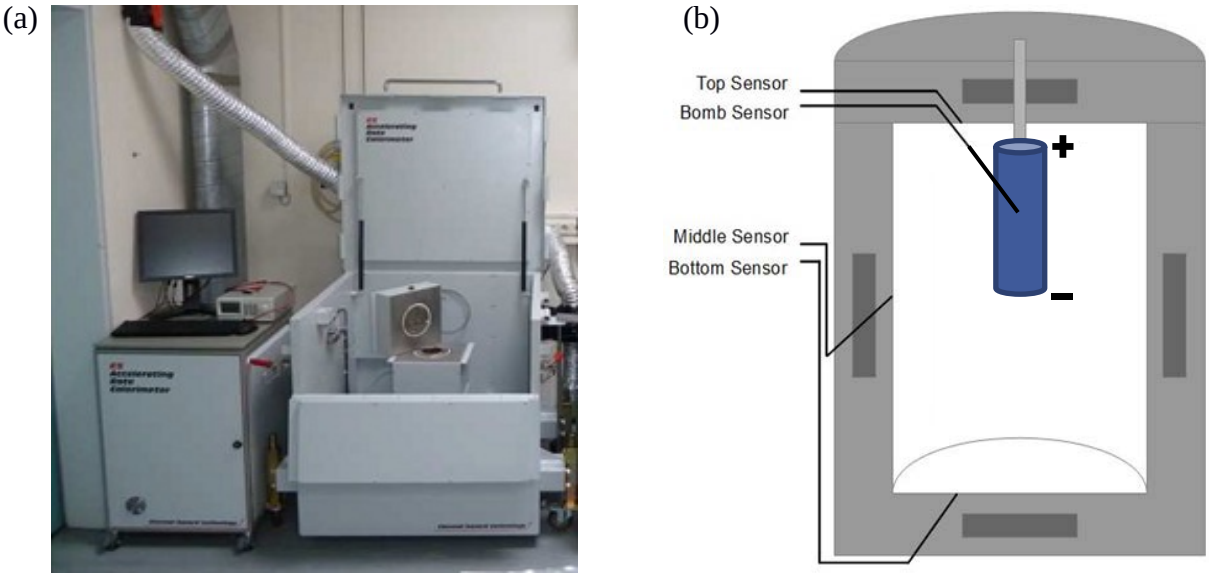

Figure 1: Accelerating Rate Calorimeter (ARC): a) Foto of es-ARC system produced by Thermal Hazard Technology and b) Schematic setup of the cell in the calorimeter chamber.

The cylindrical calorimeter chamber (diameter of 10 cm, height of 10 cm) has one heater and one thermocouple located in the lid and in the bottom; and two heaters and thermocouples (all type N) in the side wall. The tested cell is fixed on the lid of the calorimeter chamber. The calorimeter temperature is controlled by a main or so-called bomb thermocouple attached onto the surface of the cell. The heaters adjust the required temperatures depending on the measurement conditions. In the adiabatic mode the heaters in the calorimeter chamber follow immediately any change of the bomb thermocouple, thus preventing that the cell can transfer heat to the walls. All tested cells were cycled three times with the constant current constant voltage (CCCV) method, which means charging at a constant current with a rate of 1C, followed by charging with the maximal voltage until the current decreases to C/10. Afterwards, the cells were discharged with a 1C rate until the minimal voltage was reached. Finally, before the ARC test, the cells were charged to SOC 100. Following this, the tested cell was fixed on the lid of the calorimeter, as shown in Fig. 1b).

The HWS method starts in the *Heat mode* by heating up the cell in small temperature steps (here 5 K), as shown in the schematic flowchart in Fig. 2a). At the end of each step the *Wait Mode* will be activated to reach thermal equilibrium over a certain time. After reaching thermal equilibrium, the system enters *Seek Mode*, which seeks the temperature rate and ends with two possible modes - *Exotherm Mode* (adiabatic conditions) or *Heat Mode*. If the measured temperature rate is larger than the onset sensitivity (here 0.02 K/min), the system goes into *Exotherm Mode*. On the other hand, if the temperature rate is smaller, the system goes back into *Heat Mode*. If the temperature exceeds the end temperature value (here 523 K) the ARC enters the *Cool Mode*, switches off the heaters and starts to cool down by introducing pressurized air to the chamber [9]. For the Ramp Heating method, which mimics a Hot Box test, the cells were heated up continuously from 303 K to 523 K in the ARC at a constant rate of 2.5 K/min instead of a stepwise heating of the cells as in the HWS method (s. Fig. 2b).

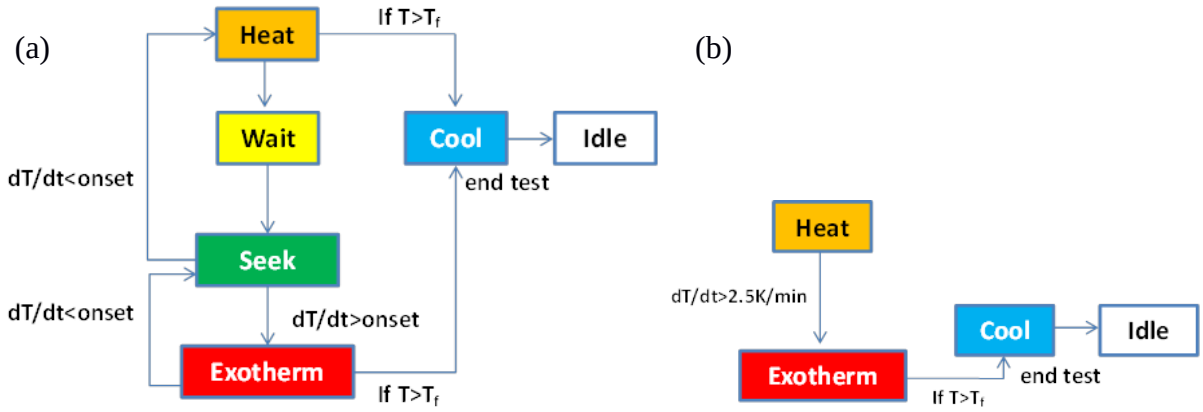

Figure 2: ARC Thermal Runaway testing methods: a) Flowchart of the heat-wait-seek (HWS) method and b) Flowchart of the Ramp Heating (RH) method.

3 Details of electrochemical-thermal model

To model the thermal behaviour of LIB the main focus is the consideration of a single cell. It is assumed that the interior of the cell is separated from the environmental air due to the battery can, so the cell can be considered as a closed system. Under general working conditions, LIB are exposed to an electrical and/or a thermal load. As consequence, heat is generated inside the cell due to several electrochemical and chemical processes. If the heat generation inside the cell is smaller than the ability of the cell to dissipate heat to the environment, the cell is in a thermally stable state. If more heat is generated in the cell than can be dissipated to the environment the cell is in a thermally unstable state. The worst case scenario in this second case is the occurrence of a thermal runaway. The critical aspect in the case of a thermal runaway is its relation to the energy conservation. With the help of the energy conservation, one is able to describe thermal characteristics like heat generation and heat dissipation.

2.1 The energy conservation

If there is no heat convection inside the LIB, the general equation for the energy conservation can be derived from Fourier's law as initial boundary problem [10] with the parabolic differential equation:

$$\rho c_p \frac{\partial T}{\partial t}(\mathbf{x}, t)\kappa \Delta T(\mathbf{x}, t) + Q_{gen}(\mathbf{x}, t) \quad (1)$$

for the temperature $T : (\mathbf{x}, t) \in \Omega \times \mathbb{R}+ \mapsto \mathbb{R}$ of the cell in K. The corresponding initial and boundary conditions are:

$$T(\mathbf{x},0)=T(\mathbf{x}), \forall\, \mathbf{x} \in \overline{\Omega}, \quad (2)$$

$$\mathbf{n} \cdot (\kappa \nabla T) = -h(T - T_{env}) - \varepsilon\sigma(T_4 - T_{env}^4), \forall \mathbf{x} \in \partial\Omega \quad (3)$$

In this framework $\mathbf{x} \in \overline{\Omega} \subset \mathbb{R}^3$ is an spatial interior or surface point of the cell and $t \in \mathbb{R}^+ := \{t \in \mathbb{R},\, t \geq 0\}$ is the time. T_{env} denotes the environmental temperature, T_0 is the initial temperature profile inside the cell at t = 0 s. It is assumed, that the initial temperature at the boundary of the cell coincides with the environmental temperature at t = 0 s. Ω denotes the interior of the battery cell, $\partial\Omega$ represents the boundary of the cell and the closure $\Omega = \Omega \cup \partial\Omega$ is the complete cell. Furthermore $\mathbf{n} \in \mathbb{R}^3$ is the outward pointing normal vector, h is the heat transfer coefficient, ε the emissivity, σ the Stefan-Boltzmann constant, ρ the density of the cell, c_p the heat capacity and κ the thermal conductivity. The solution of equation (1) describes the temperature distribution inside the cell for times $t > 0$ and all spatial points $\mathbf{x} \in \Omega$. Equation (2) represents the given initial distribution of the temperature in the LIB at t = 0s. Finally equation (3) is the heat dissipation to the environment. The first term on the right hand side of equation (3) is the heat dissipation due to convection, while the second term describes the heat dissipation due to radiation. In the inhomogeneity Q_{gen} different heat sources are included. These contributions are coming from the heat generated by reversible and irreversible thermodynamic effects, which are represented by the electrochemical heat source $Q_{el-chem}$ and from exothermic kinetic side reactions $Q_{exotherm}$:

$$Q_{gen}(\mathbf{x},t) = Q_{el-chem}(\mathbf{x},t) + Q_{exotherm}(\mathbf{x},t). \quad (4)$$

Thus, for $Q_{exotherm}$ and $Q_{el-chem}$ in equation (4) additional mathematical models must be developed.

2.2 Identifying the electrochemical heat sources

If a cell is exposed to an electric load I, heat will be generated inside the cell due to the reversible and irreversible processes in the cathode, anode and the electrolyte of the LIB. The total electrochemical heat source is then:

$$Q_{el-chem} = Q_{rev} + Q_{irrev} \quad (5)$$

$$Q_{rev} = I \cdot T \cdot \frac{\partial U_{eq}}{\partial T} \quad (6)$$

$$Q_{irrev} = I(U - U_{eq}) \quad (7)$$

The critical variables in the electrochemical heat source are the equilibrium voltage U_{eq} and the derivation of the equilibrium voltage with respect to the temperature $\partial U_{eq}/\partial T$. Due to their porous structure the cathode and the anode consist of a solid phase filled with a liquid phase that is represented by the electrolyte: Thus a model based on the porous electrode model [4] has to be applied, which represents a multi-scale multi-domain approach (MSMD). Such an approach takes the physical and geometrical structure of the LIB on the different length scales and different geometrical domains into account. The three domains of interest are identified as: (i) the particle domain, (ii) the electrode domain, and (iii) the cell domain. To every domain an associated coordinate system taking into account the corresponding length

scales and geometries are used. Charge transfer kinetics has to be solved on the electrode-electrolyte interface. The transport of the Li-ions is modelled with a diffusion mechanism and the migration and diffusion of the Li-ions through the liquid electrolyte can be evaluated. The charge balances in the solid cathode and anode as well as the liquid electrolyte are also resolved in the corresponding matrices. To determine the electrochemical heat sources one has to apply the spatial averaging theorem to the corresponding current densities and heat fluxes on each domain level. A detailed survey can be found in [11] and the references therein.

2.3 Modeling the thermal runaway and exothermic heat sources

Exothermic reaction kinetics is closely related to thermal abuse mechanisms. Several exothermic chemical reactions can occur inside a cell as the temperature rises. Consequently the heat source in the corresponding heat equation has to be extended with various exothermic reactions, for example reactions at the solid-electrolyte interface (SEI), reactions between anode resp. cathode and the electrolyte and reactions related to the decomposition of the electrolyte. This may generate heat that accumulates inside the cell and accelerates the chemical reaction between the cell components, if the heat generation rate exceeds the dissipation rate to the surroundings. External conditions for a temperature rise can be external heating, over-charging or over-discharging, high current charging, nail penetration, external short or others. In these cases a thermal runaway can occur in consequence with leakage, smoke, gas venting, flames etc., which leads to the destruction of the cells. Several authors have given models to describe abuse behaviour and thermal runaway. To describe the thermal runaway of a LIB one has to identify the main exothermic chemical reactions. Following [12, 13, 14] the general mechanism, that leads to a thermal runaway can be described with respect to rising temperature in four main stages as follows:

(1) SEI decomposition reaction: At $T > T_1$ the solid-electrolyte interface (SEI) will decompose in an exothermic reaction $\Rightarrow$ heat source Q_{sei}.

(2) Negative solvent reaction: At $T > T_2$ an exothermic reaction between the intercalated Li-ions and the electrolyte will start $\Rightarrow$ heat source Q_{ne}.

(3) Positive solvent reaction: For $T > T_3$ an exothermic reaction between the positive material and the electrolyte takes place under the evolution of oxygen inside the cell $\Rightarrow$ heat source Q_{pe}.

(4) Electrolyte decomposition: In a final exothermic reaction the electrolyte will decompose at $T > T4$ $\Rightarrow$ heat source Q_{ele}.

For these exothermic heat sources one assumes that the n independent exothermic reactions are governed by simple Arrhenius laws. Then the exothermic heat source is given as:

$$Q_{exotherm}(\mathbf{x}, t) = \sum_{i=1}^{n} Q_i(\mathbf{x}, t) \tag{8}$$

$$\text{with} \quad Q_i(\mathbf{x}, t) = c_i(\mathbf{x}, t) \cdot q_i \cdot A_i \exp\left(-\frac{E_{a,i}}{R \cdot T(\mathbf{x}, t)}\right) \tag{9}$$

where $c_i(\mathbf{x}, t)$ is the dimensionless concentration, q_i is the reaction enthalpy in J·g^{-1}, A_i is the frequency factor in 1/s, $E_{a,i}$ is the activation energy in J·mol^{-1} and R is the universal gas constant. For the simulations, it was assumed that the concentration $c_i(\mathbf{x}, t)$ is constant. In this so-called *constant fuel model* all time-spatial dynamics of the concentrations are neglected. The exothermic heat sources defined in equation (9) are thus only dependent on the temperature T, i.e. for $i \in \{sei, pe, ne, ele\}$:

$$Q_i(\mathbf{x}, t) = c_{i0} q_i A_i \exp\left(-\frac{E_{a,i}}{RT(\mathbf{x}, t)}\right) \tag{10}$$

where the index *sei* means solid-electrolyte interface (SEI) decomposition reaction, *pe* is the positive solvent reaction; *ne* represents the negative solvent reaction and *ele* the electrolyte decomposition.

4 Details of model implementation and simulation with Comsol Multiphysics

The mathematical model described in the last section represents a simple multi-scale multi-domain approach, which has been implemented in the *Battery and Fuel Cell Module* of *COMSOL Multiphysics* that is coupled to the *Heat Transfer in Solids Module*. For the simulations presented next, a cylindrical 18650 cell with $LiCoO_2$ chemistry was chosen and an axial- symmetric pseudo-2D model was implemented. From the material database in *COMSOL Multiphysics* a Li_xC_6 anode, a Li_xCoO_2 cathode and as electrolyte 1:1 EC : DEC with a $LiPF_6$ salt have been used. The internal spirally wound geometry was not resolved. From the reaction-diffusion system of the exothermic reactions inside the LIB only the additional heat sources have been used to extend the heat transport equation with additional heat sources (constant fuel model). The main physical parameters of the simulations can be found in [11]. The simulations were performed in COMSOL Multiphysics Version 5.2. For the time integration a backward differentiation formula (BDF) integration scheme was chosen with a minimum order of 1 and a maximum order of 5 using a variable step size with a maximum time step of 1s and an absolute tolerance of 0.001. Since the spatial discretisation is based on the Finite Element Method (FEM) an adaptive spatial discretisation in the three models of the particle domain, the electrode and the cell domain was used. The model of the particle domain was solved automatically in the *Battery and Fuel Cell* Module. Therefore only a spatial discretisation for the electrode domain and the cell domain was needed. The electrode domain was one-dimensional and the cell domain was modelled due to symmetry reasons in the angular direction of a cylindrical cell as two-dimensional. In the electrode domain, the maximum element size in the discretisation was chosen as 1 µm. And in total, the discretisation contained 168 elements. For the one-dimensional finite element discretisation in the electrode domain quadratic basis functions were chosen. In the cell domain the spatial discretisation was performed in the r − z-plane using 2266 triangular elements with the element size in the interval $[3.9 \cdot 10^{-4}, 8.45 \cdot 10^{-2}]$m and quadratic basis functions. To simulate the ramp heating method, an additional boundary condition was implemented, which describes the increasing environmental temperature during heating by a surface heat source $Q_{surf} = 905\ W/m^2$. This value is equivalent to a constant heating rate of 2.5 K/min.

5 Experimental Results

In Fig. 3, the HWS method (see Fig. 3a) and the Ramp Heating method (Fig. 3b) are compared. From the RH method, less information can be extracted: it can be seen that the temperature increased linearly at the beginning, and that the inflection point is around 423 K.

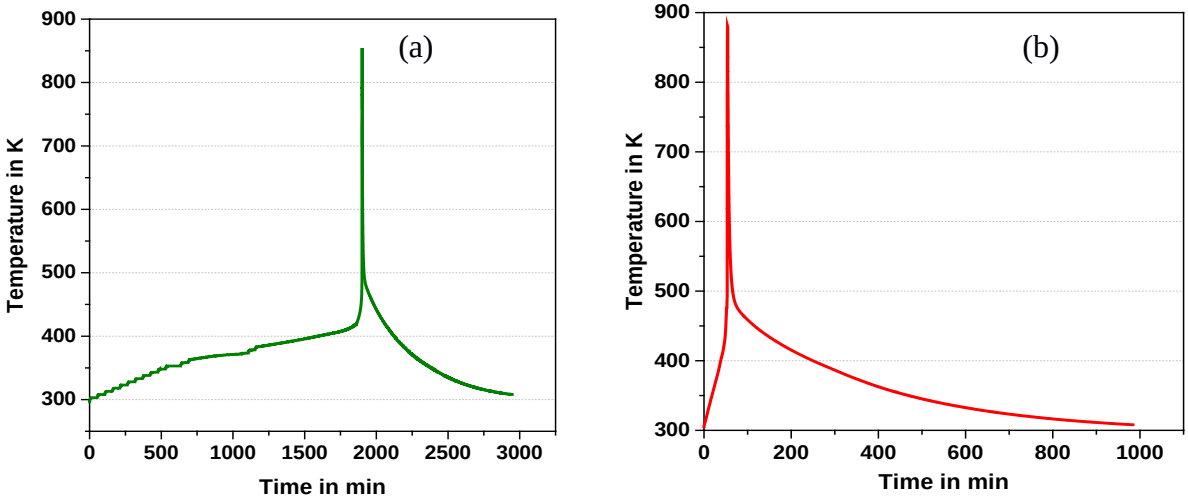

Figure 3: Comparison of measured temperature versus time curves: (**a**) Heat-Wait-Seek (HWS) method; and (**b**) Ramp Heating (RH) method [8].

On the contrast the HWS method is relatively sensitive and reveals the entire process of the thermal runaway with the different stages. At temperatures below 353 K, the cell was heated with steps of 5 K. Then at 365 K, a first exothermic reaction can be observed, where the self-heating rate is higher than 0.02 K/min. At 373 K the system switched back to *Heat mode*. Finally at 383 K, the temperature continuously increased in *Exotherm mode*, until thermal runaway occurred. After reaching a maximum temperature of more than 850 K the forced cooling by switching off the heaters at 523 K and introducing pressurized air leads to a continuous decrease of the temperature curve.

6 Simulation Results

To classify the different stages of a thermal runaway in the phase-space $\mathcal{T}$ the overall spatial mean cell temperature $\overline{\mathrm{T}}$, and their first $\mathrm{d}\overline{\mathrm{T}}/\mathrm{dt}$ and second $\mathrm{d}^2\overline{\mathrm{T}}/\mathrm{dt}^2$ time derivative have been considered.

$$\overline{\mathrm{T}}(\mathrm{t}) \coloneqq \frac{1}{\mathrm{V}}\int_{\mathrm{V}} \mathrm{T}(\mathrm{x},\mathrm{t})\mathrm{dx} \qquad (11)$$

The time evolution of the overall mean cell temperature towards the thermal runaway is given in Fig. 4. However, due to the simplification by applying the constant fuel model this simulation is not able to capture the cooling part of the curve that can be seen in the experimental curves in Fig. 3.

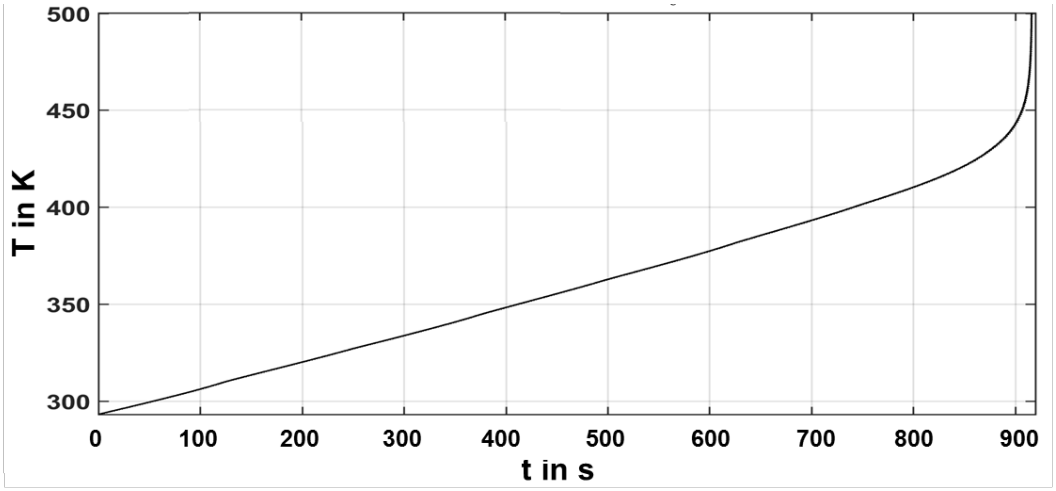

Figure 4: Simulated thermal runaway curve, when the RH method is applied.

In Fig. 5 the two-dimensional projections of the phase-space $\mathcal{T}$ for the RH method are shown. The horizontal and vertical dashed lines coincide with critical heating rates $\mathrm{d}\overline{\mathrm{T}}/\mathrm{dt}$ and temperatures $\overline{\mathrm{T}}$ as described in [13]. From Figure 5 one can identify three zones during the rise of the temperature $\overline{\mathrm{T}}$ towards the thermal runaway:

- Zone 1: Below $\overline{T} \approx 400$ K the heating rate $d\overline{T}/dt$ is bounded below a threshold $d\overline{T}/dt|_{thres,1}$ at a low level at a nearly constant rate Fig. 5a)). In Fig. 5b) the corresponding evolution of $d^2\overline{T}/dt^2$with respect to $\overline{T}$ is given.
- Zone 2: In Fig. 5a) the heating rate is rising above $\overline{T} \approx$ 400 K while the overall mean cell temperature is rising, but stays bounded below a threshold $d\overline{T}/dt|_{thres,2}$. More precisely the increase in the heating rate starts already at temperatures $\overline{T} \approx 360$ K (Fig. 5b)). The corresponding relationship between $d\overline{T}/dt$ and $d^2\overline{T}/dt^2$ is shown in Fig. 5c).

- Zone 3: Finally for temperatures $\overline{T} \geq 435$ K the heating rate $d\overline{T}/dt$ as function of the overall mean cell temperature $\overline{T}$ shows a linear increase in the semi-logarithmic plot of the Fig. 5a). This corresponds to an exponential dependence of $d\overline{T}/dt$ with respect to $\overline{T}$ i.e.

$$\frac{d\overline{T}}{dt} = a \cdot \exp\left(b \cdot \overline{T}\right), \overline{T} \geq T_0 \qquad (12)$$

where T_0 is the lower limit of the validity of this dependence, and *a*, *b* are some constants. A similar behaviour can be found for $d^2\overline{T}/dt^2$in Figure 5b). In general one can show by induction that the n^{th} time derivative of the overall mean cell temperature shows an exponential growth with respect to $\overline{T}$:

$$\frac{d^n\overline{T}}{dt^n} = a_n \cdot \exp\left(b_n \cdot \overline{T}\right), \overline{T} \geq T_{0,} n \geq 1 \quad (13)$$

with a_n, b_n some constants. This is the region where the thermal runaway starts, which is equivalent with a blow-up in the temperature curve and the time derivatives of arbitrary order. The double-logarithmic plot in the Figure 5c) shows a linear dependency between $d^2\overline{T}/dt^2$ and $d\overline{T}/dt$ in the right area of the plots. Again by induction one can show that the n^{th} time derivative $n \geq 2$ of the overall mean cell temperature shows a linear behaviour with respect to the heating rate $d\overline{T}/dt$, i.e.

$$\frac{d^2\overline{T}}{dt^2} = A \cdot \frac{dT}{dt} + B, \overline{T} \geq \overline{T}_0 \qquad (14)$$

where *A*, *B* are some constants.

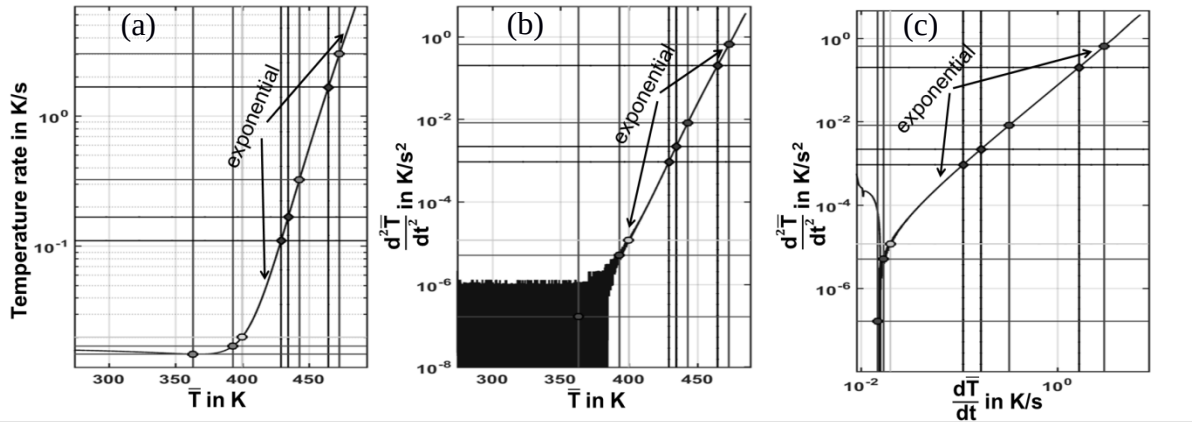

Figure 5: Two-dimensional projections of the phase-space $\mathcal{T}$ (a) $\overline{T} - d\overline{T}/dt$ -trajectory, (b) $\overline{T} - d^2\overline{T}/dt^2$-trajectory, (c) $d\overline{T}/dt - d^2\overline{T}/dt^2$-trajectory.

7 Comparison of experiments and simulation and discussion

Both in the experiments and the simulation the thermal runaway could be clearly observed. Fig. 2(a) compares the temperature rate vs. the temperature curves for the HWS and the ramp heating experiment. From the HWS curve three stages of the thermal runaway process can be distinguished. In the temperature region from 353 K to 423 K, the temperature rate is lower than 0.02 K/s. From 423 K to 473 K, the energy was released with a medium rate lower than 0.42 K/s. Above 473 K, the exothermic reactions happened in a violent way with a temperature rate over 17 K/s. On the contrast the ramp heating curve shows only the constant heating rate and an inflection point at about 423 K, where the rate starts to increase. Fig. 6(b) shows the same plot for the ramp heating simulation. When comparing it with the detailed view of the experiments in Fig. 6(c) there can be found a good quantitative agreement between experiments and simulation. In both cases the linear increase of the curves in the thermal runaway regime can be clearly

seen in the semi-logarithmic plot, which represents an exponential growth. A similar behaviour could be found for d^2T/dt^2 vs. T. This is the region where the thermal runaway starts, which is equivalent with a blow-up in the temperature curve and the time derivatives of arbitrary order. By such combined studies cooling systems of electric vehicles can be better adjusted and safety can be increased.

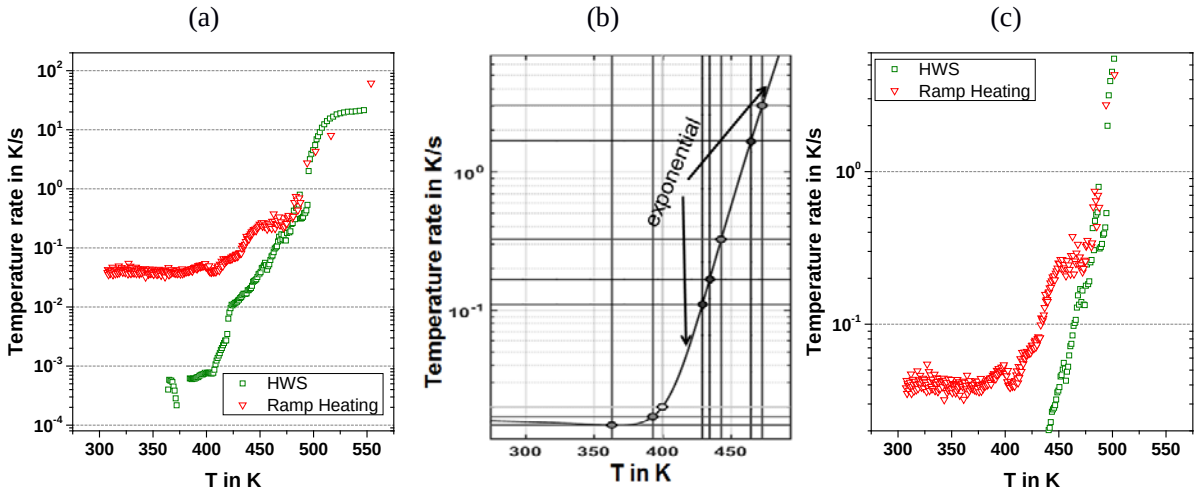

Figure 6: Comparison of temperature rate vs. temperature plots: (a) HWS and ramp heating experiment, (b) Ramp heating simulation, (c) Detailed view of (a) for easier comparison with simulation curves in (b).

8 Conclusion and outlook

For thermal abuse experiments on Li-ion cells a good quantitative agreement has been achieved between experimental and simulation results. In future experimental studies, it could be interesting to confirm the observed different stages exactly and to analyse material components after thermal runaway using post-mortem analysis by opening the cells when the experiments are stopped at the different stages. The model should then also be extended to be able to simulate the HWS method. Extensive simulations for selected temperature profiles, with the variation of certain system parameters, have demonstrated that this model can simulate the thermal runaway and that critical system parameters can be identified. Using the mean cell temperature and their first and second derivatives, a functional relationship between these variables was established. This could lead to a system for the early detection of the thermal runaway e.g. by combining temperature sensors, heat flux sensors for measuring the current temperature rate and predictive simulation, which give the Battery Management System an indication that a critical thermal event is going to happen.

Acknowledgments

This R&D project is part of the project IKEBA which was funded by the German Federal Ministry for Education and Research (BMBF) within the framework “IKT 2020 Research for Innovations” under the grant 16N12515 and was supervised by the Project Management Agency VDI | VDE | IT..

References

[1] T. Lu, C. Chiang, S. Wu, K. Chen, S. Lin, C. Wen, C. Shu, *Thermal hazard evaluations of 18650 lithium-ion batteries by an adiabatic calorimeter*, J. Therm. Anal. Calorim., 114, 1083 (2013).

[2] L. Cai, R.E. White, *Mathematical modeling of lithium ion battery with thermal effects in COMSOL Inc. Multiphysics (MP) software*, J. Power Sources 196, 5985–5989 (2011).

[3] K.J. Lee, K. Smith, A. Pesaran, G.H. Kim, *Three dimensional thermal-, electrical, and electrochemical-coupled model for cylindrical wound large format lithium-ion batteries*, J. Power Sources 241, 20–32 (2013).

[4] J. Newman, W. Tiedemann, *Porous-Electrode Theory with Battery Applications*, AIChE Journal 21 (1) (1975) 25-41.

[5] T.D. Hatchard, D.D. MacNeil, A. Basu, J.R. Dahn, *Thermal Model of Cylindrical and Prismatic Lithium-Ion Cells*, J. Electrochem. Soc. 148 A755–A761 (2001).

[6] G.H. Kim, A. Pesaran, R. Spotnitz, *A three-dimensional thermal abuse model for lithium-ion cells*, J. Power Sources 170, 476–489 (2007).
[7] P. Peng, Y. Sun, F. Jiang, *Thermal analyses of LiCoO2 lithium-ion battery during oven tests*, Heat Mass Transf. 50, 1405–1416 (2014).
[8] B. Lei, W. Zhao, C. Ziebert, A. Melcher, M. Rohde, H.J. Seifert, *Experimental analysis of thermal runaway in 18650 cylindrical cells using an accelerating rate calorimeter*, Batteries, 3 (2017) 14, doi:10.3390/batteries3020014.
[9] C. Ziebert, A. Melcher, B. Lei, W.J. Zhao, M. Rohde, H.J. Seifert, *Electrochemical-thermal characterization and thermal modeling for batteries*, in: L.M. Rodriguez, N. Omar, Eds., EMERGING NANOTECHNOLOGIES IN RECHARGABLE ENERGY STORAGE SYSTEMS, Elsevier Inc., ISBN 978032342977.
[10] J. Bebernes, D. Eberly, Mathematical Problems from Combustion Theory, Applied Mathematical Sciences Volume 83, Springer, Berlin, Germany, 1989.
[11] A. Melcher, C. Ziebert, M. Rohde, B. Lei, H.J. Seifert, Modeling and Simulation of the Thermal Runaway Behavior of Cylindrical Li-Ion Cells - Computing of Critical Parameters, Energies 9 292 (2016).
[12] P. Peng, Y. Sun, F. Jiang, *Thermal analyses of LiCoO2 lithium-ion battery during oven tests*, Heat Mass Transf. **50**, 1405–1416 (2014).
[13] T.D. Hatchard, D.D. MacNeil, A. Basu, J.R. Dahn, Thermal Model of Cylindrical and Prismatic Lithium-Ion Cells, J. Electrochem. Soc. 148 A755-A761 (2001).
[14] D.P. Abraham, E.P. Roth, R. Kostecki, K. McCarthy, S. MacLaren, D.H. Doughty, Diagnostic examination of thermally abused high-power Lithium-ion cells, J. Power Sources 161 648-657 (2006).

Authors

Dr. Carlos Ziebert, Head of the Battery Calorimeter Centre, IAM-AWP, KIT

Carlos Ziebert earned his PhD (2002) in Physics from the Saarland University, Germany. In 2002 he joined the KIT. He has more than 15 years of international R&D experience in thin film technology, modelling and thermal characterisation of materials for energy systems and more than 50 peer-reviewed articles. Since 2011 his research is focused on electrochemical and thermal characterization of Li-ion cells. He has been leader in 5 projects related to electrochemical energy storage and from 2011-2013 he was the manager of the EERA Joint Programme on Energy Storage (JPES). Currently Dr. Ziebert is the head of the KIT Battery Calorimeter Centre.

Dr. Andreas Melcher, Scientist at IAM-AWP, KIT

Andreas Melcher received his PhD in mathematics at the University Karlsruhe (TH) in 2006. From 2006 – 2013 he worked at the Institute of Materials and Processes of Karlsruhe University of Applied Sciences, at the Institute of Engineering Mechanics of KIT and the Institute for Pulsed Power and Microwave Technology (IHM) of KIT. From 2013-2017 he worked at the IAM-AWP at KIT. He has been project leader in several DFG and BMBF projects in the field of mathematical modelling, simulation and scientific programming. Since 2013 his research is focused on mathematical modelling and simulation of the thermal behaviour of Lithium-ion batteries.

Wenjiao Zhao, PhD student in Thermophysics and Thermodynamics Group, IAM-AWP, KIT

Wenjiao Zhao received her master degree in Materials Science and Engineering at the KIT in 2015. Her research interests include the experimental investigation of the pressure behaviour of lithium ion cells during thermal runaway and the properties of delithiated cathode materials, where she started her PhD thesis in 2016.

Dr. Magnus Rohde, Leader of Thermophysics and Thermodynamics Group, IAM-AWP, KIT

Magnus Rohde received his PhD at the Ruhr-University Bochum. After a post-doc period at the Nuclear Research Center in Karlsruhe he joined the scientific staff at the Institute of Materials Research. He is a member of the steering committee of the Thermophysical Working Group in Germany. Dr. Rohde is now head of the Thermodynamics and Thermophysics group. His research interests include the experimental determination and modelling of the heat transport in materials and components with a specific focus on the heat development and transport in Li-Ion cells during operation. He is also involved in the development of solid electrolytes.

Prof. Hans J. Seifert, Head of the Institute of Applied Materials - Applied Materials Physics

Hans J. Seifert received his PhD at the University of Stuttgart and the Max-Planck-Institute for Metal Research in 1993 and his habilitation in 2003. From 2006 – 2010 he was Professor at the Technical University of Freiberg. Since 2011 he is Professor for Materials Science and Engineering and Head of the IAM-AWP at the KIT. He is Associate Editor of the Journal of Phase Equilibria and Diffusion and of Calphad. Prof. Seifert has more than 20 years of international R&D experience in thermodynamics, calorimetry and thermodynamic modelling and more than 100 peer-reviewed articles.